Liquid Crystals
Publication details, including instructions for authors and subscription information:
http://www.informaworld.com/smpp/title~content=t713926090

On the influence of the Frank elasticity on the magnetic reorientation of nematic polymers

J. P. Casquilho[a]; L. N. Gonalves[a]; A. F. Martins[b]
[a] Departamento de Fisica, Faculdade de Ciĕncias e Tecnologia, Universidade Nova de Lisboa, Monte da Caparica, Portugal [b] Dep. de Ciĕncias dos Materiais; Faculdade de Ciĕncias e Tecnologia, Universidade Nova de Lisboa, Monte da Caparica, Portugal

To cite this Article Casquilho, J. P. , Gonalves, L. N. and Martins, A. F.(1996) 'On the influence of the Frank elasticity on the magnetic reorientation of nematic polymers', Liquid Crystals, 21: 5, 651 — 661
To link to this Article: DOI: 10.1080/02678299608032877
URL: http://dx.doi.org/10.1080/02678299608032877

LIQUID CRYSTALS, 1996, VOL. 21, NO. 5, 651–661

On the influence of the Frank elasticity on the magnetic reorientation of nematic polymers

by J. P. CASQUILHO†*, L. N. GONÇALVES† and A. F. MARTINS‡

†Departamento de Física, ‡Dep. de Ciências dos Materiais;
Faculdade de Ciências e Tecnologia, Universidade Nova de Lisboa,
Quinta da Torre, 2825 Monte da Caparica, Portugal

(*Received 17 July 1995; in final form 22 April 1996; accepted 24 June 1996*)

We study the influence of the anisotropy of the Frank elastic constants on the magnetic reorientation of the nematic phase of polymer liquid crystals. In the magnetic reorientation following a 90° director rotation with respect to an aligning magnetic field, a pattern of inversion walls develops which depends on the relative magnitude of the elastic constants and the magnetic coherence length. We show how this dependence can be experimentally studied by proton NMR. The transition from a homogeneous director reorientation to a distorted director reorientation is theoretically studied as a function of the rotation angle α. A critical angle of rotation α_c shows up, and we study its dependence on the anisotropies K_3/K_1 and K_3/K_2. Depending on these ratios and on the wavelength of the distortion, critical angles $45° < \alpha_c < 90°$ are predicted for materials with positive anisotropy of the magnetic susceptibility χ_a and $0° < \alpha_c < 45°$ (mod $\pi/2$) for materials with $\chi_a < 0$. Within the frame of a phase transition analogy, a Landau-like theory predicts the transition to be second order.

1. Introduction

The field induced instabilities in nematic liquid crystals have been a regularly visited subject of research over the last ten years, following the pioneering work of Brochard, Guyon and co-workers [1, 2]. Most of this research has been developed in the framework of the Fréedericksz transition in different geometries with a magnetic and/or an electric field [1–18]. Magnetic reorientational instabilities have also been studied by NMR [18–25]. In a magnetic reorientation experiment, a magnetic field is applied at an angle α to the director of a previously aligned sample. Equivalently, in the NMR experiments with polymer liquid crystals (PLC) reported here, the sample is rotated with respect to the magnetic field [19–23, 25]. For simplicity we will call α the rotation angle in referring to both cases. The subsequent evolution towards equilibrium of the director field is studied as a function of time, by optical or by NMR techniques. The experimental evidence for the field induced instabilities has been reported both for samples of low molecular weight liquid crystals (LMWLC) and PLC as a spatially periodic response to the applied field. When the sample is observed between crossed polarizers, the periodicity of the director field appears as a pattern of parallel stripes.

In standard NMR experiments, the geometry is much less defined compared with that for the case of the Fréedericksz transition, since the sample is put in a cylindrical tube without special surface treatment with a free surface. However, these experiments seem appropriate to study bulk properties, since the NMR signal is proportional to the sample volume (a few mm^3) and the effects of the boundaries reduce to distances of the order of the magnetic coherence length (a few microns). NMR magnetic reorientation experiments on nematic main chain polymer samples with $\chi_a > 0$ for angles of rotation, with respect to the field $\mathbf{H}$, of $\alpha < 45°$ and for $\alpha \cong \pi/2$ have been successfully simulated using Leslie equations for an infinite medium [19, 20, 22]. In the first case ($\alpha < 45°$), the reorientational equation corresponds to a uniform director rotation towards equilibrium, while in the second case ($\alpha \cong \pi/2$), the reorientational equation corresponds to a distorted periodic director evolution from an initial bend instability, with a flow perpendicular to the initial director $\mathbf{n}_0$, as explained in [19, 20]. There is also experimental evidence, both for Fréedericksz transition and NMR magnetic reorientation experiments, that a critical angle of rotation α_c separates the uniform director reorientation from the (instability driven) distorted director reorientation [5, 16, 23, 24].

In the first part of this work we will show that the bend reorientational equation leads to a pattern of splay–bend inversion walls. We will focus on the pattern dependence on the elastic anisotropy K_3/K_1 and on a reduced wavelength u_{max} defined below. Furthermore,

*Author for correspondence.

0267–8292/96 $12·00

we will show that NMR is a sensitive tool to study this dependence. In the second part of this work, we will investigate theoretically the transition from the homogeneous to the distorted director reorientation. The existence of a critical angle separating the two reorientation regimes and its dependence on the elastic anisotropy and the reduced wavelength of the distortion will be demonstrated.

2. Splay–bend inversion walls

The magnetic field is set perpendicular to the initial homogeneously aligned director $\mathbf{n}_0$ through a sample rotation of $\alpha \cong \pi/2$ about an axis normal to $\mathbf{n}_0$. The reorientational equation is a balance of the viscous, magnetic and elastic torques:

$$\gamma(\theta)\frac{\partial\theta}{\partial t} - \frac{1}{2}\chi_a \mathbf{H}^2 \sin 2\theta - K(\theta) = 0 \tag{1}$$

where θ is the angle between the local director $\mathbf{n}(t)$ and the initial director $\mathbf{n}_0$. In equation (1) $\gamma(\theta)$ is an effective viscosity depending on four Leslie viscosities [19, 20], and with $\mathbf{n}_0$ set along the OZ axis, the elastic torque is given by

$$K(\theta) = f(\theta)\frac{\partial^2\theta}{\partial z^2} + \frac{1}{2}\frac{\mathrm{d}f(\theta)}{\mathrm{d}\theta}\left(\frac{\partial\theta}{\partial z}\right)^2 \tag{2}$$

with

$$f(\theta) = K_1 \sin^2\theta + K_3 \cos^2\theta \tag{3}$$

The pattern of the instability generated structure is obtained through the resolution of the reorientational equation (1) in the limit $t \to \infty$ (when $\partial\theta/\partial t \to 0$). In dimensionless form, it can be written

$$[1-(1-\rho_K)\cos^2\theta]\frac{\mathrm{d}^2\theta}{\mathrm{d}u^2} + \frac{1}{2}\sin 2\theta\left[1+(1-\rho_K)\left(\frac{\mathrm{d}\theta}{\mathrm{d}u}\right)^2\right] = 0 \tag{4}$$

where u is a reduced distance:

$$u = z/\xi_1 \tag{4a}$$

ξ_1 is the splay magnetic coherence length:

$$\xi_1 = (K_1/\chi_a \mathbf{H}^2)^{1/2} \tag{4b}$$

and ρ_K is the ratio of the bend to the splay elastic constants:

$$\rho_K = K_3/K_1 \tag{4c}$$

We first look for solutions of (4) in the one constant approximation $\rho_K = 1$:

$$\frac{\mathrm{d}^2\theta}{\mathrm{d}u^2} + \frac{1}{2}\sin 2\theta = 0 \tag{5}$$

This equation, for an infinite medium, with the boundary conditions

$$\theta(0) = 0 \quad \text{and} \quad \theta(\infty) = \pi/2 \tag{6}$$

has an aperiodic solution [26]

$$\theta(u) = 2 \arctan \exp(u) - \pi/2 \tag{7}$$

corresponding to a Helfrich splay–bend wall, parallel to the field, of width defined as $2\xi_1$. Equation (5) also allows for periodic solutions. This can be easily seen noticing that this equation is identical to the equation of motion of the pendulum in reduced variables. For the pendulum we have

$$\frac{\mathrm{d}^2\phi}{\mathrm{d}t^2} = -\omega^2 \sin\phi \tag{8a}$$

and in our case we have with $\phi = 2\theta$,

$$\frac{\mathrm{d}^2\phi}{\mathrm{d}z^2} = -\xi_1^{-2}\sin\phi \tag{8b}$$

We can then import the results known from the pendulum motion [27]: equation (8 *b*) has a periodic solution with a wavelength given by

$$\lambda = 4\xi_1 K(k) \tag{9}$$

where $K(k)$ is the complete elliptic integral of the first kind [28]:

$$K(k) = \int_0^{\pi/2} \frac{\mathrm{d}x}{(1-k^2\sin^2 x)^{1/2}}, \qquad k = \sin\frac{1}{2}\phi_{\max} = \sin\theta_{\max} \tag{10}$$

where $\theta_{\max}$ is the amplitude of the distortion. From (10) we see that

$$\lim K = \pi/2, \quad \theta_{\max} \to 0 \qquad \lim K = \infty, \quad \theta_{\max} \to \pi/2 \tag{11}$$

The first limit shows, together with (9), that $\lambda \geqslant 2\pi\xi_1$. The second limit, with (9), means that a finite wavelength must correspond to an amplitude of the distortion smaller than $\pi/2$. The integral (10) is plotted as a function of $\theta_{\max}$ in figure 1.

We now turn to the general case $\rho_K \neq 1$. We define as before the wall width as $2\xi_1$. We define the quantity $u_{\max}$ as the value of u given by (4 *a*) for $z = \lambda/4$. Later we show that $u_{\max}$ is an NMR observable and that it can be simply related to the volume fraction of walls in the sample. The wavelength is given in terms of $u_{\max}$ by

$$\lambda = 4\xi_1 u_{\max} \tag{12a}$$

and we see that $u_{\max}$ is a reduced wavelength. The comparison of equations (12 *a*) and (9) suggests that the quantity $u_{\max}$ substitutes the function $K(k)$ in dealing

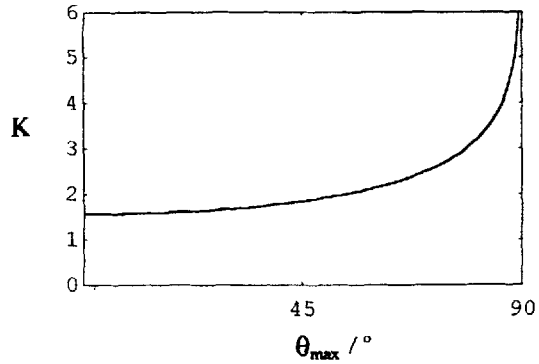

Figure 1. Plot of the integral $K(\theta_{max})$ given by equation (10). This function represents also $u_{max}(\theta_{max})$ in the case $\rho_K = 1$ (see text).

with the general case $\rho_K \neq 1$. In terms of the wave vector $\mathbf{q}$ we have the relation

$$u_{max} = \frac{\pi}{2}\frac{1}{q\xi_1} \tag{12b}$$

Equation (4) has been solved numerically by a shooting method using the Runge–Kutta and Adams–Moulton fourth order algorithms. With boundary conditions (6), we get numerical solutions which in the case $\rho_K = 1$ reduces to Helfrich walls (see curve 1 of figure 2). With periodic boundary conditions $\theta(u = 0) = \theta(u = 2u_{max}) = 0$, we get periodic solutions corresponding to a K_3/K_1 dependent pattern of splay–bend walls (see curves 2 and 3 of figure 2).

We have shown that equation (1) leads to splay–bend walls, which correspond to a pattern of parallel stripes perpendicular to the initial director. This pattern has been confirmed by optical observations on a main chain nematic PLC [20] and is in agreement with numerical results from the study of the splay Fréedericksz transition [4] which show that for high reduced magnetic fields (proportional to field × sample thickness) the stripe pattern is perpendicular to $\mathbf{n}_0$.

The experimental study of the pattern of inversion walls is conveniently made by NMR. Following [20–22], we will simulate the NMR spectral lineshape $f(\nu)$ from the spectrum of the aligned monodomain $f_0(\nu)$, assuming that the spectra are determined by dipolar interactions and using the equation

$$f(\nu) = \frac{1}{u_{max}}\int_0^{u_{max}} \frac{f_0(\nu/P_2(\cos\alpha))}{P_2(\cos\alpha)}\,du \tag{13}$$

where $P_2(\cos\alpha)$ is the second Legendre polynomial and $\alpha = \pi/2 - \theta(u)$, where u is the reduced distance (4*a*) and u_{max} is the reduced wavelength given by (12*a*), and with $\theta(u)$ given by the numerical solution of (4) with u_{max} and ρ_K as fitting parameters. The NMR spectrum of the wall pattern was taken from reference [20] and refers to a nematic thermotropic main chain polymer labelled AZA9. A simulation is shown in figure 3. The evaluation of u_{max} and ρ_K by this technique depends on the lineshape of the central part of the spectrum as explained in [22]. Poor spectra will give poor results, mainly because there can be a few pairs of u_{max} and ρ_K that give fits of similar

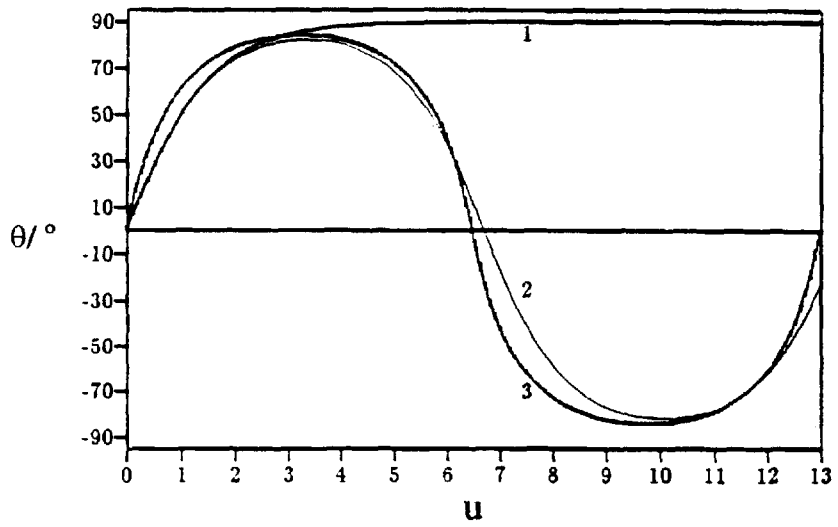

Figure 2. Splay–bend walls as numerical solutions of equation (4). This equation has been solved numerically by the shooting method, fixing the initial slope of the curve (which is related to the parameter ρ_K) and the intersection with the u axis (which is $2u_{max}$), using the Runge–Kutta and Adams–Moulton fourth order algorithms. Curve 1 is a solution with the boundary conditions (6) with $\rho_K = 1$, corresponding to a Helfrich-like wall as given by equation (7). Curves 2 and 3 correspond to periodic boundary conditions $\theta(u = 0) = \theta(u = 2u_{max}) = 0$, with $u_{max} = 3{\cdot}36$ and $\rho_K = 1$ (curve 2), $u_{max} = 3{\cdot}25$ and $\rho_K = 0{\cdot}3$ (curve 3).

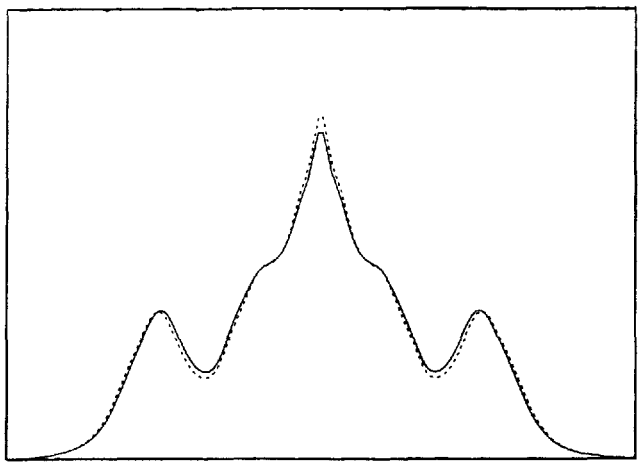

Figure 3. Simulation of the wall spectrum of polymer AZA9 with equation (13) and numerical solutions of (4): curve --- fit with $u_{max} = 3{\cdot}0$ and $\rho_K = 0{\cdot}3$.

quality, although these two parameters do not compensate each other exactly for spectral simulation purposes. In the case of the spectrum shown in figure 3, the pair ($u_{max} = 3{\cdot}0$, $\rho_K = 0{\cdot}3$) gave the best fit, but ($u_{max} = 2{\cdot}5$, $\rho_K = 0{\cdot}2$) or ($u_{max} = 3{\cdot}5$, $\rho_K = 0{\cdot}5$) gave similar results.

Once u_{max} and ρ_K are known, the measurement of the wavelength can give full information about the elastic constants K_1 and K_3, if χ_a is known, via the relations (12*a*) and (4*b*,*c*). Using the results of [20], $\lambda \cong 60\,\mu m$ and $\chi_a H^2 = 35{\cdot}5\,erg\,cm^{-3}$, we get from the above first pair (u_{max}, ρ_K) the results $K_1 = 8{\cdot}9 \times 10^{-6}$ dyne and $K_3 = 2{\cdot}7 \times 10^{-6}$ dyne, while from the second and third pairs we have, respectively, ($K_1 = 1{\cdot}3 \times 10^{-5}$ dyne, $K_3 = 2{\cdot}6 \times 10^{-6}$ dyne) and ($K_1 = 6{\cdot}5 \times 10^{-6}$ dyne, $K_3 = 3{\cdot}3 \times 10^{-6}$ dyne). These results are in good agreement with early data from spectral simulation using the time dependent equation (1) [20]. The advantage of this new method is that it allows the evaluation of the elastic constants independently of the Leslie viscosities which enter in $\gamma(\theta)$.

It is interesting to see that the volume fraction X_w of walls in the sample can be simply related to the quantity u_{max} assuming that the distribution of the wall pattern along the axis of the NMR sample tube is uniform and using equation (12*a*):

$$X_w \cong \frac{\text{wall width}}{\text{distance between walls}} = \frac{2\xi_1}{\lambda/2} = \frac{1}{u_{max}}$$

This means that $1 < u_{max} < \infty$, similarly to $K(k) \equiv u_{max}(\rho_K = 1)$ given by (10) as shown in figure 1.

3. Critical angle of rotation

In magnetic reorientation experiments as reported in [5, 16, 19, 20, 23, 24], the nematic director reorients uniformly in space for rotation angles below the critical angle α_c. Above α_c, the director reorients inhomogeneously, inducing backflow. This is a complex mechanism, ruled by the Leslie equations, where the whole set of Leslie viscosities and Frank elastic constants play an important role. Here we will only focus on the distortion of the director field once a wavevector **q** is selected. The study of the mechanism responsible for the selection of the wavevector **q** for given viscoelastic parameters and magnetic field is beyond the scope of this work. In what follows, we will assume that the system response is slow enough to validate a static analysis (see discussion of the limits of this approximation at the end of this section). For simplicity, we will consider only the planar director problem and two dimensional wavevectors. This should be a good approximation for thick samples in strong magnetic fields, since numerical results for the Fréedericksz transition [4] show that the general three-dimensional problem reduces to two dimensions for high reduced magnetic fields (proportional to field × sample thickness).

Consider a bulk nematic monodomain previously aligned with a strong magnetic field **H** and then suddenly rotated so that the uniform director $\mathbf{n}_0$ makes an angle α with **H**. Our first ansatz for the response of the out of equilibrium nematic will be a harmonic distortion along the unperturbed director $\mathbf{n}_0$, corresponding to a bend distortion. With $\mathbf{n}_0$ along the OZ axis and OY the axis of the sample rotation, we have for the distorted director

$$\mathbf{n} = (\sin\theta, 0, \cos\theta), \quad \theta = \theta_0 \sin\Omega, \quad \Omega = \mathbf{q}z \qquad (14)$$

The corresponding distortion Frank free energy density [26] is

$$f^b(\theta) = \frac{1}{2}(K_1 \sin^2\theta + K_3 \cos^2\theta)\left(\frac{d\theta}{dz}\right)^2 - \frac{1}{2}\chi_a \mathbf{H}^2 \cos^2(\theta - \alpha) \qquad (15a)$$

or

$$f^b(\Omega) = \frac{1}{2}[K_1 \sin^2(\theta_0 \sin\Omega) + K_3 \cos^2(\theta_0 \sin\Omega)]\mathbf{q}^2\theta_0^2 \cos^2\Omega - \frac{1}{2}\chi_a \mathbf{H}^2 \cos^2(\theta_0 \sin\Omega - \alpha) \qquad (15b)$$

The interesting quantity for an infinite medium is the mean free energy density per wavelength:

$$F^b = \frac{1}{2\pi}\int_0^{2\pi} f^b(\Omega)\,d\Omega \qquad (16)$$

The calculation gives the result

$$F^{b} = \frac{1}{8}\mathbf{q}^2\theta_0^2\left[K_1 + K_3 + (K_3 - K_1)\frac{J_1(2\theta_0)}{\theta_0}\right] - \frac{1}{4}\chi_a\mathbf{H}^2[1 + \cos(2\alpha)J_0(2\theta_0)] \quad (17)$$

where J_0 and J_1 are Bessel functions of the first kind (see Appendix A1). We can rewrite (17) in dimensionless form:

$$\Phi_\alpha^b(\theta_0) = \frac{1}{2}\varepsilon_1\theta_0^2 g_b(\theta_0) - [1 + \cos(2\alpha)J_0(2\theta_0)] \quad (18)$$

with

$$g_b(\theta_0) = \rho_K + 1 + (\rho_K - 1)\frac{J_1(2\theta_0)}{\theta_0} \quad (19)$$

and where $\Phi_\alpha^b(\theta_0) = 4F^b/\chi_a\mathbf{H}^2$, ρ_K is given by (4*c*) and

$$\varepsilon_1 = \frac{K_1\mathbf{q}^2}{\chi_a\mathbf{H}^2} \quad (20)$$

is a ratio of an elastic to magnetic energy. This quantity is easily related to the reduced wavelength u_{max} with the help of equations (12*b*) and (4*b*):

$$\varepsilon_1 = \left(\frac{\pi}{2}\frac{1}{u_{max}}\right)^2 \quad (21)$$

From the plot of the bend potential $\Phi_\alpha^b(\theta_0)$ for several values of the rotation angle α, with u_{max} (or ε_1) and ρ_K as parameters, a critical angle of rotation α_c shows up, separating two different ranges of α, as shown in figure 4 for the polymer AZA9: for $\chi_a > 0$, for values of α up to α_c the minimum of $\Phi_\alpha^b(\theta_0)$ lies at $\theta_0 = 0$, thus showing that a deformation is not favoured; for α greater than a value α_c, which depends on the parameters u_{max} (or ε_1) and ρ_K, the minimum of $\Phi_\alpha^b(\theta_0)$ lies at $\theta_0 \neq 0$, meaning that the distortion can be amplified. The first angle of rotation for which the minimum of the potential lies at $\theta_0 \neq 0$ is taken as the critical angle α_c. For AZA9 we get a coarse grained $\alpha_c = 48°$ by inspection of $\Phi_\alpha^b(\theta_0)$.

We get a finer analysis by minimisation of the bend potential (18) with respect to the amplitude θ_0, giving the equation (see Appendix A2)

$$\varepsilon_1\theta_0 h_b(\theta_0) + 2\cos(2\alpha)J_1(2\theta_0) = 0 \quad (22)$$

where

$$h_b(\theta_0) = \rho_K + 1 + (\rho_K - 1)J_0(2\theta_0) \quad (23)$$

and with ε_1 given by (21). Equation (22) is a balance of an elastic and a magnetic term. Depending on the values for α, this equation has only the trivial solution $\theta_0 = 0$ or two more solutions $\pm\theta_0 \neq 0$. This can be easily seen by solving (22) graphically: plotting the first (elastic) term and minus the second (magnetic) term as a function

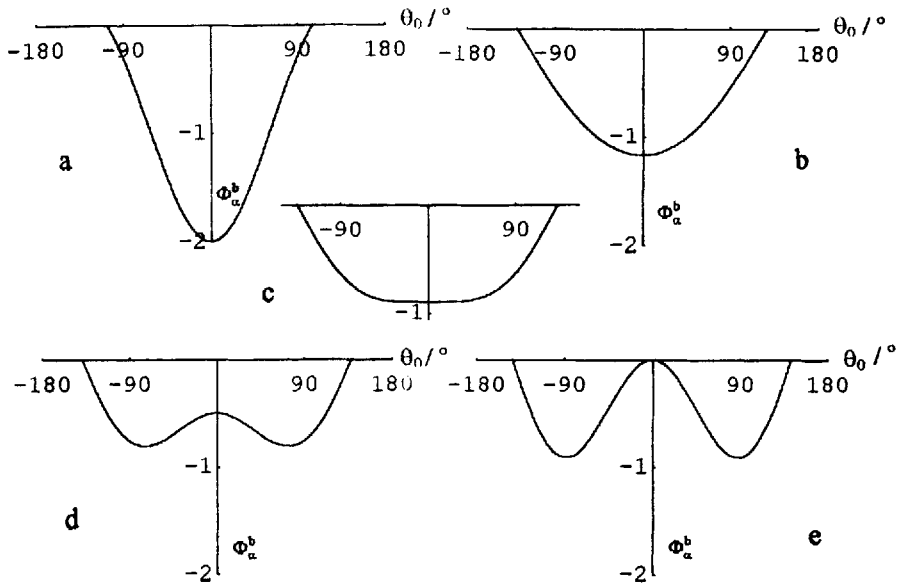

Figure 4. Plot of the bend potential $\Phi_\alpha^b(\theta_0)$ given by (18) (only the negative part is shown and the physical range of θ_0 lies between $-90°$ and $90°$) for several values of the rotation angle α, with $u_{max} = 3{\cdot}0$ and $\rho_K = 0{\cdot}3$ (obtained in § 2 for the polymer AZA9 for which $\chi_a > 0$): (*a*) $\alpha = 0°$; (*b*) $\alpha = 40°$; (*c*) $\alpha = 48°$; (*d*) $\alpha = 60°$; (*e*) $\alpha = 90°$. This figure reminds us of a second order phase transition, with α as the external parameter and θ_0 as the order parameter. An analysis based on a phase transition analogy is presented in § 4. A critical angle of rotation α_c separates the symmetrical 'phase' with $\theta_0 = 0$ from the unsymmetrical 'phase' with $\theta_0 \neq 0$ (see also figure 5). The above values of the parameters u_{max} and ρ_K give $\alpha_c = 48°$, determined by inspection of $\Phi_\alpha^b(\theta_0)$.

of θ_0 (for $\theta_0 \geqslant 0$ for simplicity), there is a nontrivial solution if the two curves intersect at some $\theta_0 \neq 0$, as can be seen in figure 5, again for AZA9. The first angle of rotation which produces such a solution is taken as the critical angle, giving for AZA9 a finer grained $\alpha_c = 47{\cdot}5^\circ$ (not shown in the figure). No solutions with $\theta_0 \neq 0$ are found for $\chi_a > 0$ and $\alpha < 45^\circ$, or for $\chi_a < 0$ and $\alpha > 45^\circ$. In the case $\chi_a > 0$, solutions of (22) are found with α_c up to $\approx 90^\circ$, and with α_c down to $\approx 0^\circ$ for $\chi_a < 0$. This is in agreement with experimental results for lyotropic low molecular weight nematics with negative χ_a, where measurement of the critical angle gives 20° for DSCG in water [5] and 25° for DSI in water [16]; results for lyotropic polymer nematics with positive χ_a ($PBDG/CH_2Cl_2$) give critical angles up to 50° for different polymer concentrations [23] and results for 5CB ($\chi_a > 0$) give $\alpha_c = 85^\circ$ [24]. Focusing on the case $\chi_a > 0$, from the plot of the elastic term of (22) for a given u_{max}, *increasing* ρ_K increases the initial slope of the curve, and thus *increases* α_c; a similar analysis shows that for a given ρ_K, *decreasing* u_{max} *increases* α_c. A picture of α_c as a function of these parameters can be seen in figure 6 (*a*) with the help of a phase transition analogy presented below.

The second ansatz for the distortion of the nematic director will be a splay–bend mode, replacing in (14) for Ω

$$\Omega = q_x x + q_z z \tag{24}$$

Following similar calculations as for the bend case, the reduced mean free energy density can be written as

$$\Phi_\alpha^{sb}(\theta_0) = \frac{1}{2}\varepsilon_1 \theta_0^2 [g_b(\theta_0) + \rho_q^2 g_s(\theta_0)] - [1 + \cos(2\alpha) J_0(2\theta_0)] \tag{25}$$

with $g_b(\theta_0)$ given by (19) and

$$g_s(\theta_0) = \rho_K + 1 - (\rho_K - 1)\frac{J_1(2\theta_0)}{\theta_0} \tag{26}$$

$$\rho_q = q_x/q_z \tag{27}$$

and with ε_1 now related to u_{max} by

$$\varepsilon_1 = \left(\frac{\pi}{2}\frac{1}{u_{max}}\right)^2 \frac{1}{1+\rho_q^2} \tag{28}$$

In the limit of zero splay, $\rho_q \to 0$, equation (25) reduces to (18) and (28) to (21) for the bend case as expected. The plot of the splay–bend potential $\Phi_\alpha^{sb}(\theta_0)$ given by (25–28) gives curves similar to those shown in figure 4, now with the extra parameter ρ_q. Inspection of $\Phi_\alpha^{sb}(\theta_0)$ shows that for the parameters of AZA9, the critical angle α_c is shifted for higher values with increasing ρ_q: $\rho_q = 0{\cdot}5$ gives $\alpha_c = 49^\circ$, $\rho_q = 1$ gives $\alpha_c = 51^\circ$, all these values being consistent with results from magnetic reorientation experiments for this PLC [31]. The analysis hereafter will show, however, that α_c can also decrease with increasing ρ_q. This can be seen by minimising the splay–bend potential $\Phi_\alpha^{sb}(\theta_0)$ with respect to θ_0, giving

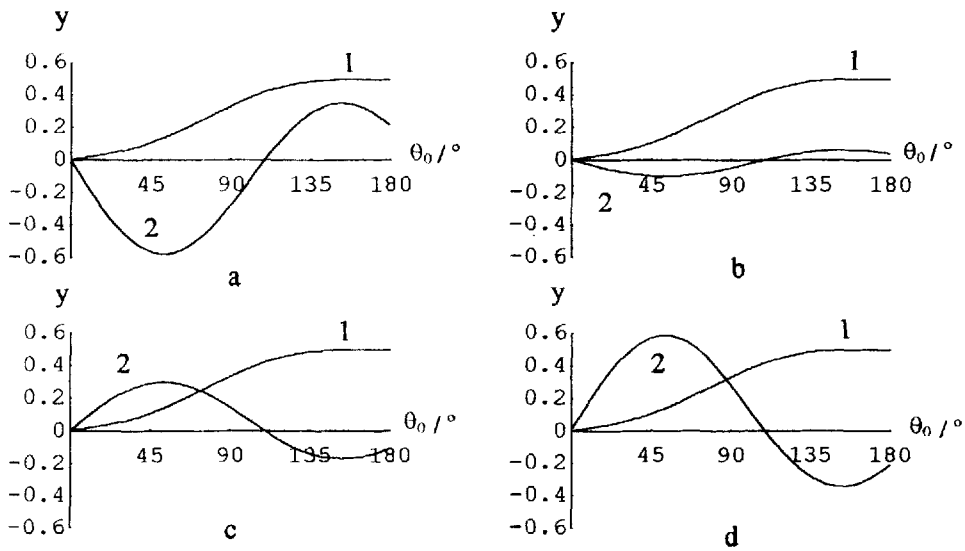

Figure 5. The equation (22) is solved graphically: curve 1 is the first (elastic) term $y = \varepsilon_1 \theta_0 h_b(\theta_0)$ for the same parameters of figure 4 ($\chi_a > 0$, $\rho_q = 0$, $u_{max} = 3{\cdot}0$ and $\rho_K = 0{\cdot}3$) and curve 2 is minus the second (magnetic) term $y = -2\cos(2\alpha)J_1(2\theta_0)$ for the following values of the rotation angle: (*a*) $\alpha = 0^\circ$; (*b*) $\alpha = 40^\circ$; (*c*) $\alpha = 60^\circ$; (*d*) $\alpha = 90^\circ$. (*a*) and (*b*) show only the solution $\theta_0 = 0$, while (*c*) and (*d*) show another solution at $\theta_0 \neq 0$. For $\chi_a < 0$ the magnetic term in (22) is negative and the figure should be read backwards.

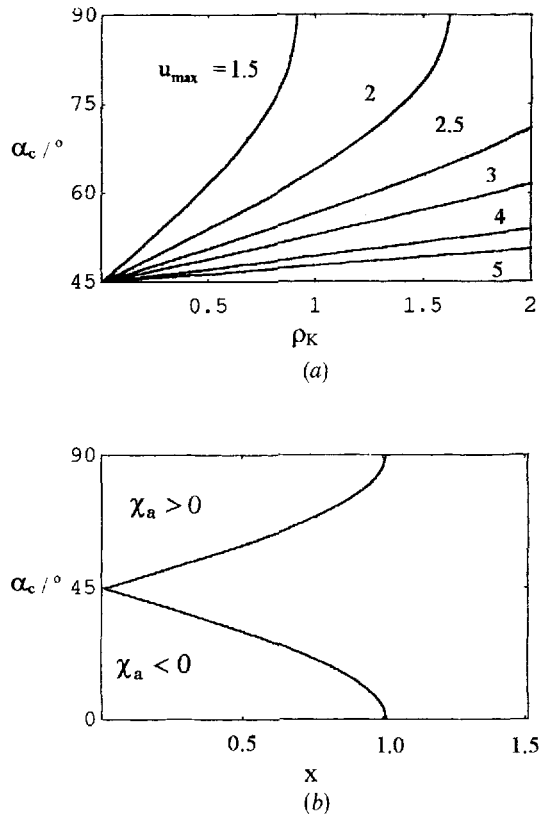

Figure 6. Phase diagrams for the bend potential $\Phi_\alpha^b(\theta_0)$. (*a*) From (42*a*) with $\chi_a > 0$ we get α_c as a function of ρ_K with u_{max} as a parameter. (*b*) From (42*b*) we get α_c as a function of $x = K_3 q_z^2/\chi_a H^2$; at $x = 1$ the curve goes to infinity for $\chi_a > 0$ and to zero for $\chi_a < 0$.

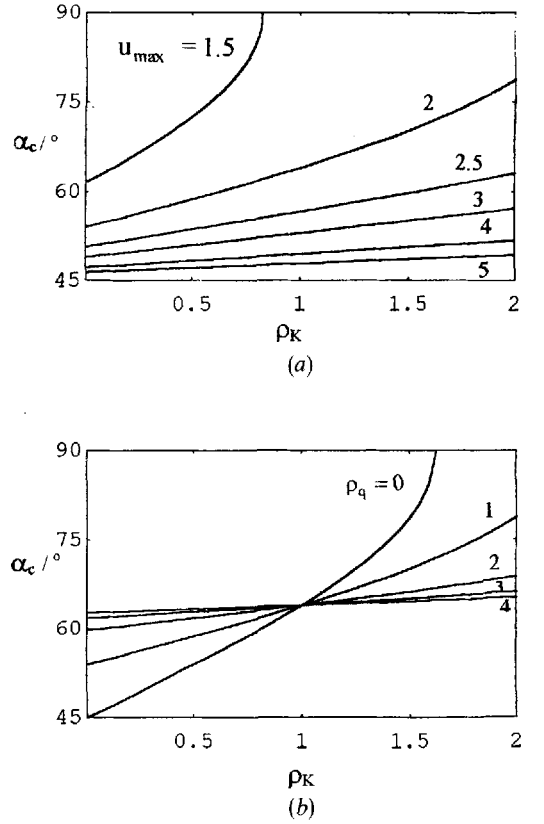

Figure 7. Phase diagrams from equation (43) for the splay–bend potential $\Phi_\alpha^{sb}(\theta_0)$ with $\chi_a > 0$ in the (ρ_K, α_c) plane: (*a*) with u_{max} as a parameter and $\rho_q = 1$; (*b*) with ρ_q as a parameter and $u_{max} = 2$, showing that α_c *increases* with increasing ρ_q for $0 < \rho_K < 1$ and *decreases* with increasing ρ_q for $\rho_K > 1$.

the equation

$$\varepsilon_1 \theta_0 [h_b(\theta_0) + \rho_q^2 h_s(\theta_0)] + 2\cos(2\alpha) J_1(2\theta_0) = 0 \tag{29}$$

where

$$h_s(\theta_0) = \rho_K + 1 - (\rho_K - 1) J_0(2\theta_0) \tag{30}$$

and with $h_b(\theta_0)$ and ε_1 given by (23) and (28), respectively. Following the same graphical method as for the bend case, we observe that α_c *increases with increasing* ρ_q for $0 < \rho_K < 1$, and *decreases with increasing* ρ_q for $\rho_K > 1$. This again can be pictured with the help of a phase transition analogy as shown in figure 7 (*b*). This is in agreement with the known result that bend distortions are favoured for $K_3/K_1 < 1$ (in the infinite chain limit, $K_3/K_1 \to 0$ [29] and splay is forbidden), while for $K_3/K_1 > 1$ splay is favoured.

Our third ansatz for the distortion will be a twist–bend mode, corresponding to an out of plane component for **q**, which now gives for Ω in (14):

$$\Omega = q_y y + q_z z \tag{31}$$

Following the same steps as before, the calculation for the reduced mean free energy density gives

$$\Phi_\alpha^{tb}(\theta_0) = \varepsilon_2 \theta_0^2 + \Phi_\alpha^b(\theta_0) \tag{32}$$

where $\Phi_\alpha^b(\theta_0)$ is the bend potential given by (18) and

$$\varepsilon_2 = \frac{K_2 q_y^2}{\chi_a \mathbf{H}^2} \tag{33}$$

is a twist elastics to magnetic energy ratio arising from the introduction of the out of plane component of the wavevector. This ratio is related to the reduced wavelength u_{max} by

$$\varepsilon_2 = \left(\frac{\pi}{2}\frac{1}{u_{max}}\right)^2 \frac{(K_2/K_1)\rho_q^2}{1 + \rho_q^2} \tag{34}$$

where now ρ_q is given by

$$\rho_q = q_y/q_z \tag{35}$$

Equation (32) with the relations (18), (19), (28), (34) and (35) gives for the twist–bend potential

$$\Phi_\alpha^{tb}(\theta_0) = \left(\frac{\pi}{2}\frac{1}{u_{max}}\right)^2 \frac{1}{1+\rho_q^2}\theta_0^2\left[\frac{1}{2}g_b(\theta_0) + \frac{K_2}{K_1}\rho_q^2\right] - [1+\cos(2\alpha)J_0(2\theta_0)] \quad (36)$$

In the limit of zero twist, $\rho_q \to 0$, equation (36) reduces to (18). The plot of $\Phi_\alpha^{tb}(\theta_0)$ again gives curves similar to those shown in figure 4, showing a critical angle depending on four parameters: u_{max}, $\rho_K = K_3/K_1$, K_2/K_1 and $\rho_q = q_y/q_z$. Minimising the potential (36) with respect to θ_0 gives the equation

$$\left(\frac{\pi}{2}\frac{1}{u_{max}}\right)^2 \frac{1}{1+\rho_q^2}\theta_0\left[h_b(\theta_0) + 2\frac{K_2}{K_1}\rho_q^2\right] + 2\cos(2\alpha)J_1(2\theta_0) = 0 \quad (37)$$

with $h_b(\theta_0)$ given by (23). Following the same graphical method as for the preceding cases, we conclude that, for given u_{max}, ρ_q and ρ_K, α_c increases with increasing K_2/K_1. The influence of ρ_q is harder to understand than the splay–bend case, since the elastic term in (37) depends on two elastic ratios, K_3/K_1 and K_2/K_1: while for $K_2/K_1 < x_c$, where x_c is a critical ratio of K_2/K_1, α_c *decreases* with increasing ρ_q, for $K_2/K_1 > x_c$, α_c *increases* with increasing ρ_q, and x_c increases with increasing K_3/K_1 with the law $x_c \propto K_3/K_1$. Thus both anisotropies play a role in the twist–bend instability driven reorientation by affecting the critical angle. A study based on a phase transition analogy (see §4) helps to clarify the ρ_q dependence of α_c: for $K_3/K_2 < 1$, α_c increases with increasing ρ_q (increasing the twist component of the distortion), while for $K_3/K_2 > 1$, α_c decreases with increasing ρ_q (see figure 8 (*a*)), showing that bend distortions are favoured for $K_3/K_2 < 1$, while for $K_3/K_2 > 1$ twist is favoured.

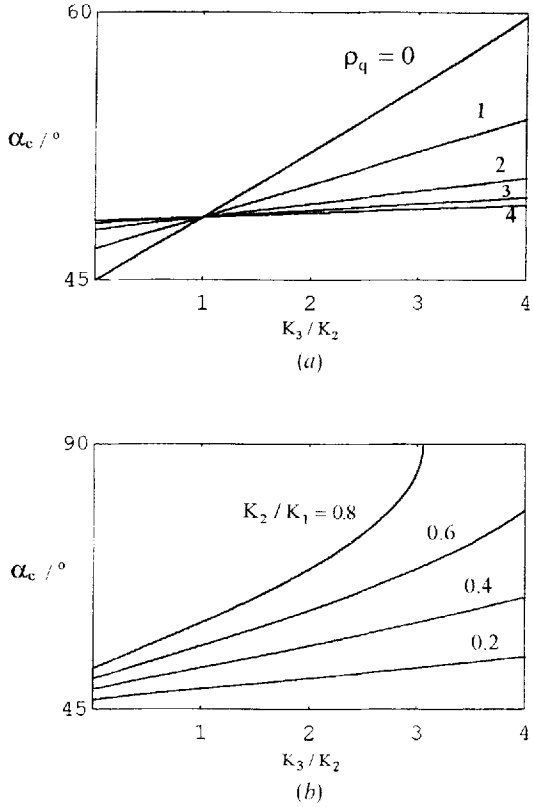

Figure 8. Phase diagram corresponding to equation (44) in the $(K_3/K_2, \alpha_c)$ plane: (*a*) with ρ_q as a parameter, for $u_{max} = 2$ and $K_2/K_1 = 0{\cdot}2$, showing that α_c *increases* with increasing ρ_q for $K_3/K_2 < 1$ and *decreases* with increasing ρ_q for $K_3/K_2 > 1$; (*b*) with K_2/K_1 as a parameter, for $u_{max} = 2$ and $\rho_q = 1$.

4. Results from a phase transition analogy

The plot of the potentials $\Phi_\alpha^{sb}(\theta_0)$ and $\Phi_\alpha^{tb}(\theta_0)$, as shown in figure 4 for the special case $\rho_q = 0$, remind us of a second order phase transition, with the angle α playing the role of the external parameter and the value of the amplitude θ_0, corresponding to the minimum of the potential, Θ, the role of the order parameter. As in second order phase transitions [30], the order parameter vanishes continuously at $\alpha = \alpha_c$: for $\chi_a > 0$, Θ continuously decreases by decreasing the rotation angle, going to zero for $\alpha \to \alpha_c$. The symmetrical 'phase' with $\Theta = 0$ is unstable for $\alpha < \alpha_c$. The amplitude θ_0 plays the same role of an order parameter as for the aperiodic magnetic Fréedericksz transition, which is also analogous to a second order phase transition [26]. This analogy suggests the use of the Landau theory of second order phase transitions as an approximation to study the behaviour of the system near the critical angle. This theory should give a good approximation since $\Theta \to 0$ when $\alpha \to \alpha_c$. Following the usual Landau approach, we expand the appropriate potential in a power series of θ_0 up to the fourth order.

$$\Phi_\alpha(\theta_0) = \Phi_0 + \frac{a}{2}\theta_0^2 + \frac{b}{4}\theta_0^4 + O(\theta_0) \quad (38)$$

with

$$\Phi_0 = -(1+\cos 2\alpha) \quad (39)$$

In (38), the odd-order terms vanish identically due to the symmetry of the problem (θ_0 is physically equivalent to $-\theta_0$). For the bend potential $\Phi_\alpha^b(\theta_0)$ given by (18), we have

$$a = 2(\varepsilon_1\rho_K + \cos 2\alpha) \quad (40)$$

$$b = \varepsilon_1(1-\rho_K) - \cos 2\alpha \quad (41)$$

The transition points are determined by the equation $a=0$. At this point, $\alpha=\alpha_c$. The coefficient a can be written, using equation (21), as a function of the parameters u_{max} and ρ_K, and the equation becomes

$$\cos 2\alpha_c = -\left(\frac{\pi}{2}\frac{1}{u_{max}}\right)^2 \rho_K \qquad (42\,a)$$

or, using (20) with $q \equiv q_z$

$$\cos 2\alpha_c = -\frac{K_3 q_z^2}{\chi_a \mathbf{H}^2} \qquad (42\,b)$$

From (42 *a*) we get lines of transition points in the (ρ_K, α_c) plane with u_{max} as a parameter, as shown in figure 6 (*a*). From equation (42 *b*) we get a phase diagram in the $(K_3 q_z^2/\chi_a \mathbf{H}^2, \alpha_c)$ plane as shown in figure 6 (*b*). This equation tells us that, in the Landau approximation, the important quantity at the transition point is the ratio of the (bend) elastic to the magnetic energy. At the transition point, this equation implies that $\chi_a > 0 \Rightarrow \alpha_c > 45°$, and $\chi_a < 0 \Rightarrow \alpha_c < 45°$. From figure 6 (*b*) we can see that in the case $\chi_a > 0$ the condition for $\alpha_c < 90°$ is $\chi_a \mathbf{H}^2 > K_3 q_z^2$. For the parameters of the polymer AZA9, this gives a critical field $\mathbf{H}_c = 4{\cdot}6$ kG. The actual magnetic reorientation experiment with this sample was performed under a field of 21·4 kG, well above $\mathbf{H}_c$.

The transition at $a=0$ is second order if $b>0$ and first order if $b<0$. For $\chi_a > 0$ and $\rho_K < 1$, or $\chi_a < 0$ and $\rho_K > 1$, b is always positive at the transition point, where $\alpha = \alpha_c$. This should be the case for polymers with long flexible chains ($\rho_K < 1$) and $\chi_a > 0$, or for LMWLC with $\rho_K > 1$ and $\chi_a < 0$. To investigate the possibility $b<0$ in the two other cases, we analyse the tricritical point defined by $a=b=0$. This equation gives $\varepsilon_1 = 0$, which by (20) means that the tricritical point is attained asymptotically at vanishingly small K_1 or $\mathbf{q}$. This means that the transition is always second order.

Similar conclusions are reached from the analysis of the splay–bend and twist–bend cases, as expected on purely physical grounds. We give only the results leading to figures 7 and 8. For the splay–bend case, at the transition point, we get from the equation $a=0$ with $\rho_q = q_x/q_z$:

$$\cos 2\alpha_c = -\left(\frac{\pi}{2}\frac{1}{u_{max}}\right)^2 \frac{\rho_q^2 + \rho_K}{\rho_q^2 + 1} \qquad (43)$$

The phase diagram from (43) in the (ρ_K, α_c) plane is shown in figure 7, with u_{max} as a parameter in figure 7 (*a*) and with ρ_q as a parameter in figure 7 (*b*) (see discussion following equation (29)). For the twist–bend case, the equation $a=0$ with $\rho_q = q_y/q_z$ becomes

$$\cos 2\alpha_c = -\left(\frac{\pi}{2}\frac{1}{u_{max}}\right)^2 \frac{K_2/K_1}{\rho_q^2 + 1}\left(\frac{K_3}{K_2} + \rho_q^2\right) \qquad (44)$$

Figure 8 shows the phase diagram corresponding to equation (44) in the $(K_3/K_2, \alpha_c)$ plane with (*a*) ρ_q as a parameter (see discussion following equation (37)) and (*b*) K_2/K_1 as a parameter.

5. Discussion

We can get an estimation of the expected range of values for the critical angle α_c. We focus on the case $\chi_a > 0$ and start with $\rho_q = 0$. The critical angle increases with increasing ρ_K and with decreasing u_{max}, as shown in figure 6. We will first estimate a minimum value for this latter parameter. By inspection of figure 1 (which gives u_{max} for the case $\rho_K = 1$), we choose for this value $u_{max} \cong 2$. From equation (12 *a*), we get the corresponding minimum wavelength $\lambda_{min} \cong 8\xi_1$. For polymers, we take a strong field $\mathbf{H} = 20$ kG, $\chi_a \approx 10^{-7}$ (CGS) and $K_1 \approx 10^{-5}$ dyne cm. This gives from (4 *b*), $\xi_1 \cong 5\,\mu$m and we get $\lambda_{min} \cong 40\,\mu$m. We choose for a maximum value $u_{max} \cong 20$, corresponding to $\lambda_{max} \cong 400\,\mu$m. For flexible chains, $\rho_K < 1$ and choosing $0{\cdot}3 < \rho_K < 0{\cdot}7$ we get from equation (22) $45° < \alpha_c < 57°$ (for a picture, in the Landau approximation, the reader should refer to figure 6 (*a*)), setting an upper value for α_c consistent with experimental results for flexible polymers [23, 25, 31]. Adding a splay component to the distortion of the director field up to $\rho_q = 1$, from equation (25), increases the estimated upper value of α_c to $\approx 60°$ (for hard rods $\rho_K > 1$ and α_c would decrease) (for a picture, the reader may refer to figure 7). Adding a twist component will decrease α_c, since $K_3/K_2 > 1$ is always expected (a picture is given in figure 8 (*a*)). For LMWLC, we take $K_1 \approx 10^{-6}$ dyne cm and $\chi_a \approx 10^{-7}$ (CGS), which gives for a field $\mathbf{H} = 20$ kG $\xi_1 \cong 2\,\mu$m and $\lambda_{min} \cong 16\,\mu$m, and for a field $\mathbf{H} = 2$ kG $\xi_1 \cong 16\,\mu$m and $\lambda_{min} \cong 130\,\mu$m. Taking $1 < \rho_K < 2$, from equation (22) with $u_{max} = 2$, α_c can go up to $\approx 90°$ (a picture is given in figure 6 (*a*)). The critical angle of rotation reported for 5CB [24] is 85° for working fields $\mathbf{H} = 2$ kG. For this material $\rho_K \cong 1{\cdot}4$ [33] and from equation (22) for $\alpha_c = 85°$ we get $u_{max} = 1{\cdot}88$ (see figure 6 (*a*)), which gives, from (12 *a*) with $\xi_1 \cong 16\,\mu$m, $\lambda \cong 120\,\mu$m, of the order of our estimation for λ_{min} for a field of 2 kG. Wavelengths of this magnitude are found for 5CB in the electrically driven splay Fréedericksz transition [14], while $\lambda \approx 15\,\mu$m are found in the periodic deformed hybrid alignment of the nematic cell of 5CB [34] for cell thickness less than $0{\cdot}15\,\mu$m. Since in this case the role of the field is formally played by the cell thickness [34], this seems to correspond to the strong

field behaviour in our problem. Adding a splay or a twist component will only decrease α_c since $\rho_K > 1$ and $K_3/K_2 > 1$. Optical measurements of the wavelength and ρ_q in a sample during a magnetic reorientation experiment, together with the measurement of α_c, are of course necessary to check whether these results are quantitatively correct. In this case, equations (29) or (37), via the measurement of α_c and of λ and ρ_q by optical techniques, can provide u_{max} and ρ_K (and K_1 and K_3 as explained at the end of §2) without making use of the NMR spectra simulation technique. In the case $\chi_a < 0$, a description in terms of u_{max} is no longer adequate since ξ_1 becomes complex, but the prediction of our model that in this case α_c is in the range 0°–45° is consistent with the results for α_c reported in the literature (see discussion following equation (22)).

Although our model seems to work qualitatively well both for PLC and LMWLC, our static study of the critical angle is probably a poor approximation for LMWLC, with short relaxation times (seconds or milliseconds), and should be a better approximation for PLC where, due to their high viscosities, τ_0 is orders of magnitude higher than the relaxation times for LMWLC, and increases rapidly with the degree of polymerisation (minutes to hours) [18–23, 25, 32]. Although arguments based only on elastic energy are incomplete, numerical results for the splay Fréedericksz transition [4] indicate that the bend distortion is mediated almost entirely by the bend restoring force, none of the viscosities having much effect on it. When the bend distortion is the leading contribution, which should be the case in the bulk for high fields [4], equation (22), or the Landau approximation (42 *a*), should thens give reasonable results.

6. Conclusions

In the first part of this work, we have shown that the bend reorientational equation (1) leads to a pattern of splay-bend walls, and we have studied its dependence on the ratio K_3/K_1 and on the reduced wavelength u_{max} (12 *a*). We have also shown that with appropriate NMR experiments we can get this elastic ratio and u_{max} and, finally, that with the measurement of the wavelength we can get both K_1 and K_3.

In the second part of this work, we have shown that the minimisation of a distortion Frank free energy can explain the existence of a critical angle separating the uniform director magnetic reorientation regime from the distorted director reorientation regime. We have shown evidence for the dependence of this critical angle on the elastic anisotropy and u_{max}, thus allowing for the calculation of values for α_c using the NMR experimental results obtained in the first part. We have used different trial distortion wavevectors to study the dependence of α_c on the elastic ratios. This dependence is simple to visualise with the help of a second order phase transition analogy, where the angle of rotation plays the role of the external parameter and the value of the amplitude of the distortion plays the role of the order parameter. For a splay–bend mode, we conclude that α_c increases with increasing splay component of the distortion for $K_3/K_1 < 1$ and decreases with increasing splay for $K_3/K_1 > 1$. For a twist–bend mode, α_c increases with increasing twist component of the distortion for $K_3/K_2 < 1$, and decreases with increasing twist for $K_3/K_2 > 1$. Depending on these ratios, critical angles $45° < \alpha_c < 90°$ are predicteds for materials with positive anisotropy of the magnetic susceptibility χ_a and $0° < \alpha_c < 45°$ (mod $\pi/2$) for materials with $\chi_a < 0$, in agreement with published data.

The authors wish to thank Dr F. Volino for helpful comments. This work was partly financed by JNICT of Portugal under research contract PBIC/C/CEN/1049/93 and by the EU under HCM-Network CHRX-CT93-0282.

Appendix

(A1) The calculation of (16) with (15 *b*) is easily done with the help of normal trigonometric relations from which we get the result

$$F^b = \frac{1}{8}(K_1 + K_3)\mathbf{q}^2\theta_0^2 + \frac{1}{4}(K_3 - K_1)\frac{1}{2\pi}I_1 - \frac{1}{4}\chi_a\mathbf{H}^2\left(1 + \frac{\cos 2\alpha}{2\pi}I_2 + \frac{\sin 2\alpha}{2\pi}I_3\right)$$

with

$$I_1 = \int_0^{2\pi} \cos(2\theta_0 \sin\Omega)\cos^2\Omega \, d\Omega,$$

$$I_2 = \int_0^{2\pi} \cos(2\theta_0 \sin\Omega) \, d\Omega,$$

$$I_3 = \int_0^{2\pi} \sin(2\theta_0 \sin\Omega) \, d\Omega.$$

These integrals are evaluated with the help of tables of integrals as found in [35 (*a*)]. The integral I_1 is evaluated in four steps. Putting $2\theta_0 = z$, we get

$$\int_0^{\pi/2} \cos(z\sin\Omega)\cos^2\Omega \, d\Omega = \frac{\pi}{2}\frac{1!!}{z}J_1(z) = \frac{\pi}{2}\frac{J_1(z)}{z}$$

$$\int_{\pi/2}^{\pi} \cos(z\sin\Omega)\cos^2\Omega \, d\Omega = \int_0^{\pi/2} \cos(z\sin(\Omega + \pi/2))\cos^2(\Omega + \pi/2) \, d\Omega$$

$$= \int_0^{\pi/2} \cos(z\cos\Omega)\sin^2\Omega\,\mathrm{d}\Omega$$

$$= \frac{\pi^{1/2}}{z}\Gamma\left(\frac{3}{2}\right)J_1(z) = \frac{\pi}{2}\frac{J_1(z)}{z}$$

and similarly we get the results for the two other steps, giving

$$I_1 = 2\pi\frac{J_1(z)}{z}$$

Using a similar method for I_2 we get

$$I_2 = \int_0^{\pi} \cos(z\sin\Omega)\,\mathrm{d}\Omega + \int_0^{\pi} \cos(z\sin(\Omega+\pi))\,\mathrm{d}\Omega$$

$$= 2\int_0^{\pi} \cos(z\sin\Omega)\,\mathrm{d}\Omega = 2\pi J_0(z)$$

and for I_3

$$I_3 = \int_0^{\pi} \sin(z\sin\Omega)\,\mathrm{d}\Omega + \int_0^{\pi} \sin(z\sin\Omega+\pi)\,\mathrm{d}\Omega = 0$$

Putting these results in the above expression for F^b we get (17).

(**A2**) Equation (22) with (23) is obtained by differentiating (18) with respect to θ_0, putting $2\theta_0 = z$ and using [35(*b*)]:

$$\frac{\mathrm{d}}{\mathrm{d}z}[zJ_1(z)] = zJ_0(z) \quad \text{and} \quad \frac{\mathrm{d}}{\mathrm{d}z}J_0(z) = -J_1(z)$$

References

[1] (*a*) Brochard, F., Pieranski, P., and Guyon, E., 1972, *Phys. Rev. Lett.*, **28,** 1681; (*b*) Pieranski, P., Brochard, F., and Guyon, E, 1973, *J. Phys.*, **34,** 35.

[2] Guyon, E., Meyer, R., and Salan, J., 1979, *Mol. Cryst. liq. Cryst.*, **54,** 261.

[3] (*a*) Lonberg, F., Fraden, S., Hurd, A., and Meyer, R. B., 1984, *Phys. Rev. Lett.*, **52,** 1903; (*b*) Lonberg, F., and Meyer, R. B., 1985, *Phys. Rev. Lett.*, **55,** 718.

[4] (*a*) Hurd, A. J., Fraden, S., Lonberg, F., and Meyer, R. B., 1985, *J. Phys.*, **46,** 905; (*b*) Fraden, S., Hurd, A. J., Meyer, R. B., Cahoon, M., and Caspar, D. L. D., 1985, *J. Phys. (Paris) Colloq.*, **46,** C3-85.

[5] Hui, Y., Kuzma, M., San Miguel, M., and Labes, M., 1985, *J. chem. Phys.*, **83,** 288.

[6] (*a*) Kuzma, M., 1986, *Phys. Rev. Lett.*, **57,** 349; (*b*) Rose, D., and Kuzman, M., 1986, *Mol. Cryst. liq. Cryst.*, **4,** 39.

[7] Miraldi, E., Oldano, C., and Strigazzi, A., 1986, *Phys. Rev. A*, **34,** 4348.

[8] (*a*) Kini, U., 1986, *J. Phys.*, **47,** 693; (*b*) 1991, *Liq. Cryst.*, **10,** 597.

[9] (*a*) McClymer, J., and Labes, M., 1987, *Mol. Cryst. liq. Cryst.*, **144,** 275; (*b*) McClymer, J., Labes, M., and Kuzma, M., 1988, *Phys. Rev. A*, **37,** 1388.

[10] San Miguel, M., and Sagués, F., 1987, *Phys. Rev. A*, **36,** 1883.

[11] Frisken, B., and Palffy-Muhoray, P., 1989, *Phys. Rev. A*, **39,** 1513.

[12] Srajer, G., Fraden, S., and Meyer, R. B., 1989, *Phys. Rev. A*, **39,** 4828.

[13] Rey, A. D., and Denn, M. M., 1989, *Liq. Cryst.*, **4,** 409.

[14] (*a*) Buka, A., and Kramer, L., 1992, *J. Phys. II France*, **2,** 315; (*b*) 1992, *Phys. Rev. A*, **45,** 5624.

[15] Galatola, P., Oldano, C., and Rajteri, M., 1994, *Phys. Rev. E*, **49,** 1458.

[16] Golovanov, A. V., and Kaznacheev, A. V., 1994, 15th ILLC, Budapest.

[17] Kilian, A., 1994, *Phys. Rev. E*, **50,** 3774.

[18] Schwenk, N., and Spiess, H. W., 1993, *J. Phys. II France*, **3,** 865.

[19] Martins, A. F., Esnault, P., and Volino, F., 1986, *Phys. Rev. Lett.*, **57,** 1745.

[20] Esnault, P., Casquilho, J. P., Volino, F., Martins, A. F., and Blumstein, A., 1990, *Liq. Cryst.*, **7,** 607.

[21] Casquilho, J. P., Esnault, P., Volino, F., Mauzac, M., and Richard, H., 1990, *Mol. Cryst. liq. Cryst.*, **180B,** 343.

[22] Gonçalves, L. N., Casquilho, J. P., Figueirinhas, J., Cruz, C., and Martins, A. F., 1993, *Liq. Cryst.*, **14,** 1485.

[23] Filas, R. W., 1978, *Mesomorphic Polymers and Polymerization in Liquid Crystalline Media*, edited by A. Blumstein, ACS Symposium Series 74 (Washington DC: ACS), Chap. II.

[24] Gotzig, H., Grunenberg-Hassanein, S., and Noack, F., 1994, *Z. Naturforsch.*, **49a,** 1179.

[25] Hughes, J. R., Luckhurst, G. R., and Picken, S. J., 1994, 15th ILLC, Budapest.

[26] de Gennes, P. G., 1975, *The Physics of Liquid Crystals* (Oxford: Clarendon Press).

[27] Sommerfeld, A., 1964, *Classical Mechanics* (Academic Press).

[28] Hancock, H., 1958, *Elliptic Integrals* (New York: Dover).

[29] Meyer, R. B., 1982, *Polymer Liquid Crystals*, edited by A. Cifferi, W. R. Krigbaum and R. B. Meyer (New York: Academic Press), Chap. 6.

[30] (*a*) Landau and Lifshitz, 1980, *Statistical Physics*, Part 1 (Pergamon Press); (*b*) Huang, K., 1987, *Statistical Mechanics*, 2nd edition (Wiley).

[31] Esnault, P., 1988, PhD thesis, Université Joseph Fourier, Grenoble.

[32] Klein, T., Jun, H. X., Esnault, P., Blumstein, A., and Volino, F., 1989, *Macromolecules*, **22,** 3731.

[33] (*a*) Madhusudana, N. V., and Pratibha, R., 1982, *Mol. Cryst. liq. Cryst.*, **89,** 249; (*b*) Skarp, K., Lagerwall, S. T., and Stebler, B., *ibid.*, **60,** 215.

[34] Sparavigna, A., Lavrentovich, O., and Strigazzi, A., 1994, *Phys. Rev. E*, **49,** 1344.

[35] Gradshtein, I. S., and Ryzhik, I. M., 1994, *Tables of Integrals, Series and Products*, 5th edition (Academic Press), (*a*) pp. 441–442 and 947; (*b*) *p.* 979.